Articles

X-ray Crystallographic Structure of the Angiogenesis Inhibitor, Angiostatin, Bound to a Peptide from the Group A Streptococcal Surface Protein PAM[†,‡]

Sara E. Cnudde,[§] Mary Prorok,[||] Francis J. Castellino,[||] and James H. Geiger*[,⊥]

Department of Biochemistry, Michigan State University, East Lansing, Michigan 48824, Department of Chemistry and Biochemistry and W. M. Keck Center for Transgene Research, University of Notre Dame, Notre Dame, Indiana 46556, and Department of Chemistry, Michigan State University, East Lansing, Michigan 48824

Received May 9, 2006; Revised Manuscript Received July 28, 2006

ABSTRACT: The crystal structure of the human Pg-derived angiogenesis inhibitor, angiostatin, complexed to VEK-30, a peptide from the group A streptococcal surface protein, PAM, was determined and refined to 2.3 Å resolution. This is the first structure of angiostatin bound to a ligand and provides a model of the interaction between Pg and streptococcal-derived pathogenic proteins. VEK-30 contains a "through-space isostere" for C-terminal lysine, wherein Arg and Glu side chains, separated by one helical turn, bind within the bipolar angiostatin kringle 2 (K2) domain lysine-binding site. VEK-30 also makes several contacts with K2 residues that exist outside of the canonical LBS and are not conserved among the other Pg kringles, thus providing a molecular basis for the selectivity of VEK-30 for K2. The structure also shows that Pg kringle domains undergo significant structural rearrangement relative to one another and reveals dimerization between two molecules of angiostatin and VEK-30 related by crystallographic symmetry. This dimerization, which exists only in the crystal structure, is consistent with the parallel coiled-coil full-length PAM dimer expected from sequence similarities and homology modeling.

A critical reaction in the generation of the fibrinolytic response is the production of Pm[1] from the activation of the zymogen, Pg (*1*). Pm catalyzes the proteolysis of the fibrin network, resulting in the dissolution of blood clots (*2*, *3*). Conversion of Pg to Pm results from cleavage of the Arg561−Val562 peptide bond by Pg activators. Cleavage at this site in Pg results in the formation of two-chain Pm, which is composed of a heavy chain and light chain linked by two disulfide bonds. The heavy chain consists of the N-terminal "finger domain" followed by five consecutive homologous triple disulfide-bonded kringle domains. The light chain possesses the C-terminal serine protease catalytic unit (Figure 1A) (*4*).

Kringle modules have been shown to be protein recognition units in virtually all cases where a function has been identified. Many of these kringles display an affinity for C-terminal lysine residues on proteins and for small molecules such as EACA that mimic C-terminal lysines (*5*−*7*). Their binding modes for lysine-like ligands have been extensively studied structurally and by site-directed mu-

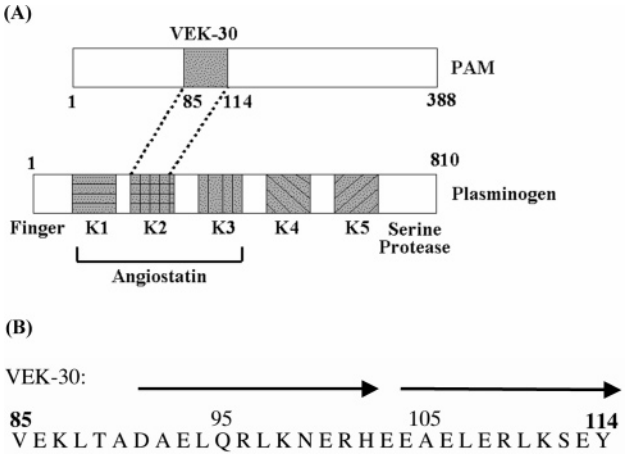

FIGURE 1: VEK-30 binds to Pg-K2. (A) Pg consists of an N-terminal finger domain followed by five consecutive homologous triple disulfide-bonded kringle domains and a C-terminal serine protease catalytic domain. The angiogenesis inhibitor angiostatin encompasses Pg-K1−3. VEK-30 is an internal 30-residue helical peptide fragment of streptococcal surface protein PAM. The VEK-30 helical peptide binds only to the Pg-K2 domain. (B) Peptide sequence of VEK-30 using PAM numbering. Arrows above the sequence indicate the two direct repeats. Note that the second direct repeat is truncated and its terminal residue was changed from Arg to Tyr.

[†] Supported by Grants GR-179 (085P100549) from the Michigan Economic Development Corp. (to J.H.G.), NIH Grant HL13423 (to F.J.C.), and NIH Grant GM0638947 (to J.H.G.).

[‡] The coordinates have been deposited in the Protein Data Bank as entries 2DOH and 2DOI.

* To whom correspondence should be addressed: Department of Chemistry, Michigan State University, East Lansing, MI 48824. Telephone: (517) 355-9715, ext. 234. Fax: (517) 353-1793. E-mail: geiger@cem.msu.edu.

[§] Department of Biochemistry, Michigan State University.

[||] University of Notre Dame.

[⊥] Department of Chemistry, Michigan State University.

[1] Abbreviations: Pg, plasminogen; Pm, plasmin; tPA, tissue-type plasminogen activator; μPA, urinary-type plasminogen activator; K, kringle; EACA, ϵ-aminocaproic acid; LBS, lysine binding site; PAM, Pg-binding group A streptococcal M-like protein; glu-Pg, full-length Pg; NTD, Pg N-terminal domain; SK, streptokinase.

10.1021/bi060914j CCC: $33.50
Published on Web 08/25/2006

tagenesis. The specific region responsible for ligand binding is the LBS. The LBS is bipolar with a cationic and anionic center that stabilizes the carboxyl and amino group of a C-terminal lysine residue (*8*−*11*). Between the two charged regions of the binding site is a hydrophobic region consisting of two aromatic residues that act as forceps for the intervening hydrophobic methylene chain of the C-terminal lysine. Pg-K1, -K4, and -K5 all show a reasonably high affinity for EACA, while Pg-K2 has a significantly lower affinity for EACA. Pg-K3 displays no affinity for any of the C-terminal lysine mimics (*12*). However, specific and high-affinity interactions between Pg kringle domains and proteins lacking C-terminal lysines have also been identified. These include tetranectin (*13*−*15*), which binds to Pg-K4, and the streptococcal surface protein PAM (*16*−*19*), which binds to Pg-K2. A ligand for Pg-K3 has yet to be identified.

The interaction between the C-terminal lysines of degrading fibrin and the lysine binding kringles of Pm or Pg serves to localize Pg to fibrin, thereby promoting continued proteolytic dissolution of the fibrin by Pm (*20*). The five Pg kringle domains have an additional regulatory function involving mediation of a dramatic conformational change (*21*, *22*). The full-length Pg (glu-Pg) exists as a tightly compact structure in the presence of Cl^- and is relatively inactive toward activation by Pg activators (*19*, *21*, *23*−*25*). This compact conformation depends, at least in part, on interactions between Pg-K5 and the NTD, since recombinant Pg bearing LBS mutations in K5 or N-terminal lysine substitutions exist only in the extended conformation (*26*).

The group A streptococcal surface protein PAM, a 43 kDa member of the M protein family, binds Pg-K2 with high affinity (*27*). M and M-like proteins account for several interactions between group A streptococci and plasma proteins and are known to act as virulence factors by inhibiting phagocytosis (*27*, *28*). In fact, PAM is required for infection by several streptococcal strains (*29*, *30*). It acts by localizing Pm to the bacterial surface, inhibiting fibrin encapsulation during infection. Pm then catalyzes both extracellular matrix and fibrin degeneration, thwarting bacterial encapsulation during infection. M and M-like proteins are thought to be highly related structurally, consisting of a continuous α-helix encompassing most of the structure, with a membrane-binding domain on the N-terminus. The continuous α-helices then dimerize, forming extended parallel coiled-coil structures that extend tens of angstroms from the cell surface. These M protein protrusions are easily visualized in EM projections (*31*). A region of PAM, spanning amino acids 91−116, contains two direct repeat sequences and is responsible for Pg binding by PAM. VEK-30, an α-helical peptide derived from residues 85−113 of PAM containing the first and most of the second direct repeat, possesses a high-affinity binding site for Pg-K2 (K_d = 460 nM) (*17*−*19*, *27*), even though it does not contain a C-terminal lysine residue (Figure 1B). VEK-30 specifically binds Pg-K2, having no measurable affinity for any of the other isolated Pg kringle domains. The crystal structure of Pg-K2, mutated to contain an upregulated lysine binding site, bound to VEK-30, demonstrates a novel kringle LBS interaction, where the C-terminal lysine is mimicked by argininyl and glutamyl side chain residues displaced by almost one helical turn (*19*). This arrangement of residues is named a "through-space isostere for C-terminal lysine".

Angiostatin is an internal fragment of Pg containing the first three or four kringle modules (Figure 1A) (*32*, *33*). It was one of the first angiogenesis inhibitors to be identified. Angiogenesis is critical for the growth of most solid tumors, as a blood supply must be recruited to stimulate significant growth (*34*, *35*). For this reason, intense interest has been focused on angiogenesis inhibitors for use as potential anticancer agents. Although the function of angiostatin in angiogenesis inhibition is uncertain, agents containing Pg-K1−3, -K1−4, and -K1−5 show potent anti-angiogenic and/or antitumor growth activity in animal models. These fragments, as well as individual kringle modules, are also inhibitory toward endothelial cell migration and/or proliferation in vitro. Later studies showed that angiostatin corresponding to K1−3 engenders all the determinants responsible for maximal inhibition of cell proliferation and motility (*36*).

To further understand kringle domain function and kringle domain specificity, angiostatin bound to the VEK-30 peptide was crystallized and its three-dimensional structure determined from two independent crystal forms, a $P6_122$ form and a $P6_1$ form. The angiostatin−VEK-30 structure is the first example of an interaction between a multiple-kringle protein and a biologically relevant ligand to be visualized at atomic resolution. Furthermore, as the only existing structure of an angiostatin−ligand complex, it provides a model at atomic resolution for testing the genesis of anti-angiogenic activity following angiostatin−ligand binding.

MATERIALS AND METHODS

Crystallization of the Angiostatin−VEK-30 Complex. Human angiostatin containing K1−3 was expressed in *Pichia pastoris* and purified as described previously (*37*). The VEK-30 peptide was synthesized and purified as previously described (*19*). Crystals of the angiostatin−VEK-30 complex were grown at room temperature by hanging-drop vapor diffusion; 1 μL of a protein solution containing 15 mg/mL angiostatin in 0.15 M NaCl, along with a 5-fold molar excess of VEK-30, was admixed with 3 μL of a reservoir solution containing 20% PEG 8000, 0.1 M potassium phosphate (dihydrate), and 5% dioxane and equilibrated over the reservoir solution. Diamondlike crystals appeared in 1 day and continued to increase in size for 2−3 weeks.

Collection of Intensity Data. The crystals were briefly soaked in a solution of 22% PEG 8000, 0.1 M potassium phosphate (dihydrate), 5% dioxane, and 30% glycerol at room temperature and flash-frozen by immersion in liquid N_2. Data were collected at the Advanced Photon Source (APS) IMCA-CAT 17-ID beamline at Argonne National Laboratory to a resolution of 2.0 Å, and data were processed and scaled using the HKL suite of programs (*38*). The crystal−detector distance was 270 mm, and 200° of data were collected with an oscillation of 0.5°. The crystal parameters and data collection statistics of the angiostatin−VEK-30 complex are listed in Table 1. The space group was $P6_122$ with one molecule in the asymmetric unit.

Structure Determination and Refinement. The structure was determined by molecular replacement using AMoRe and the structures of K1 and K2 from human angiostatin as search models (PDB entry 1KIO) (*39*). A translation search with K2 gave one solution, and a translation search with K1 after fixing the K2 translation solution also yielded one solution.

Table 1: Data Collection and Refinement Statistics for the Angiostatin−VEK-30 Complex

data collection		
space group	$P6_122$	$P6_1$
cell dimensions		
a, *b*, *c* (Å)	58.4, 58.4, 391.0	58.8, 58.8, 389.2
α, β, γ (deg)	90.0, 90.0, 120.0	90.0, 90.0, 120.0
resolution (Å)	2.0 (2.07−2.3)[a]	3.0 (3.20−3.04)[a]
R_{merge}	9.1 (30.8)[a]	8.4 (31.2)[a]
I/σ	45.12 (4.8)[a]	12.38 (3.02)[a]
completeness (%)	80.2 (78.7)[a]	78.5 (97.1)[a]
redundancy	4.8	5.7
refinement		
resolution (Å)	15−2.3	20−3.0
no. of reflections	15842	12432
R_{work}/R_{free}	20.85/25.45	20.17/29.56
no. of atoms		
protein	1525	3064
ligand/ion	12	0
water	321	0
mean *B*-factor (Å^2)	25.591	35.457
rms deviation		
bond lengths (Å)	0.014	0.023
bond angles (deg)	1.583	2.593

[a] Data for the highest-resolution shell are in parentheses.

The crystal packing of K2 and K1 was consistent with the location of K2 and K1 in the structure. This solution had a correlation factor of 41.9 and an *R* value of 44.2%, after rigid body refinement. Fixing the positions of angiostatin K1 and K2 and calculating an electron density map revealed density corresponding to the VEK-30 helix. The same electron density map revealed density connecting K1 and K2. Even after K1, K2, and VEK-30 had been fixed, rotation and translation searches performed using human angiostatin K3 as a search model (PDB entry 1KIO) were unsuccessful. After refinement of K1, K2, and VEK-30, an electron density map revealed density for two residues in the K2−K3 linker peptide, residues T244 and T245, but no electron density was ever seen downstream of residue T245. No electron density was seen for C297 of K3 at the inter-kringle K2−K3 disulfide bond. When C297 was built into the structure, negative density was calculated for residue C297 and increases in *R* and R_{free} were observed. This indicated that residues 246−333 encompassing K3 are highly flexible in this structure. The refinement parameters are listed in Table 1. The overall structure of the complex is shown in Figure 2A. An example of the $2F_o - F_c$ map contoured at 1σ is shown in Figure 2B.

Heavy atom soaks were performed on angiostatin−VEK-30 complex crystals using 5 mM $Pt(C_5H_5N)_2Cl_2$ [*cis*-dichloro-bis(pyridine) platinum(II)]. After being soaked for 24 h, the crystal was back-soaked in its cryoprotectant solution. The crystal was flash-frozen by immersion in liquid N_2. Data were collected at the DND-CAT 5-ID beamline at the APS to a resolution of 2.8 Å. The crystal−detector distance was 200 mm, and 70° of data were collected with an oscillation of 0.5°. The data were processed and scaled using the HKL suite (*40*) in space group $P6_1$. Detailed data statistics are listed in Table 1. Automated heavy atom searches using SOLVE failed to locate heavy atom positions (*41*). The cause for the change in space group was not identified. Molecular replacement using CCP4 and the $P6_1$-22 structure as a model yielded two translation solutions with correlations of 46.6 and 73.6 and *R* values of 43.2 and 31.2%, respectively (*42*). These two solutions represented the two molecules of K1, K2, and VEK-30 in the asymmetric unit of the $P6_1$ crystal form. Molecular replacement using K3 of angiostatin (PDB entry 1KIO) as a model produced no solution. An electron density map was calculated, and density for residues T244 and T245 of the K2−K3 linker was seen as in the $P6_122$ structure. No density was seen after residue T245. However, density was seen at the inter-kringle K2−K3 disulfide bond (C169−C297) for C297 of K3 for only one of the molecules in the asymmetric unit (Figure 2C). Residues P296 and K298 were then built into corresponding density in the K3 disulfide region. However, no density was seen beyond K298 or before P296. Refinement statistics are listed in Table 1. All model building was done using TURBO-FRODO, and the refinement and map calculations were carried out using CNS and CCP4 (*42*, *43*). Group *B* factor refinement was used for both structures.

The X-ray intensity data used to determine and refine the crystal structure are summarized in Table 1. The asymmetric unit of the $P6_122$ crystal form contains one angiostatin−VEK-30 complex, while the $P6_1$ crystal form that resulted from Pt(II) soaking contains a complete angiostatin−VEK-30 dimer in the asymmetric unit. The Ramachandran plot of the structure contained 138 non-glycine, non-proline residues (78.3%) in the most favored regions and 17.4% in the additionally allowed regions with E163 and E165 in the disallowed region.

Analytical Ultracentrifugation. Sedimentation equilibrium experiments were performed in a Beckman XL-I analytical ultracentrifuge operated in absorbance mode (280 nm) at 20 °C. Angiostatin was dissolved in 100 mM sodium phosphate (pH 7.4) to a final concentration of 13 μM. For experiments conducted in the presence of VEK-30, a concentrated stock solution of VEK-30 was introduced to afford an angiostatin:VEK-30 molar ratio of 1:5. Samples were rotated at speeds of 14 000 and 18 000 rpm. The partial specific volume of angiostatin (0.706 mL/g) was calculated from its amino acid composition. The data were analyzed using the sedimentation analysis software supplied by Beckman. The experimentally derived molecular weights represent the average of the fits from duplicate scans acquired at the two rotor speeds that were employed.

RESULTS

Overall Structure of the Angiostatin−VEK-30 Complex. In comparison to the unbound form of angiostatin, no electron density was detected for any of the residues of Pg-K3 (residues C256−C333) in the angiostatin−VEK-30 complex [gel electrophoresis showed the full-length angiostatin to still be intact (data not shown)]. Additionally, electron density is absent for most of the residues in the K2−K3 inter-kringle peptide (residues P246−Q255). However, the remaining residues of the Pg-K1 and Pg-K2 domains are well-ordered and exist in a relatively extended orientation with essentially no interactions between them. There are also very few interactions between either Pg-K1 or Pg-K2 and the linker peptide that connects the two domains (Figure 2A). Electron density for the VEK-30 peptide is absent for N-terminal residues Val85−Lys87 and C-terminal residues K111−Y114 (Figure 1B). Of the remaining 23 residues, 20 correspond to approximately five turns of a well-defined α-helix that is approximately 30 Å long (Figure 2A).

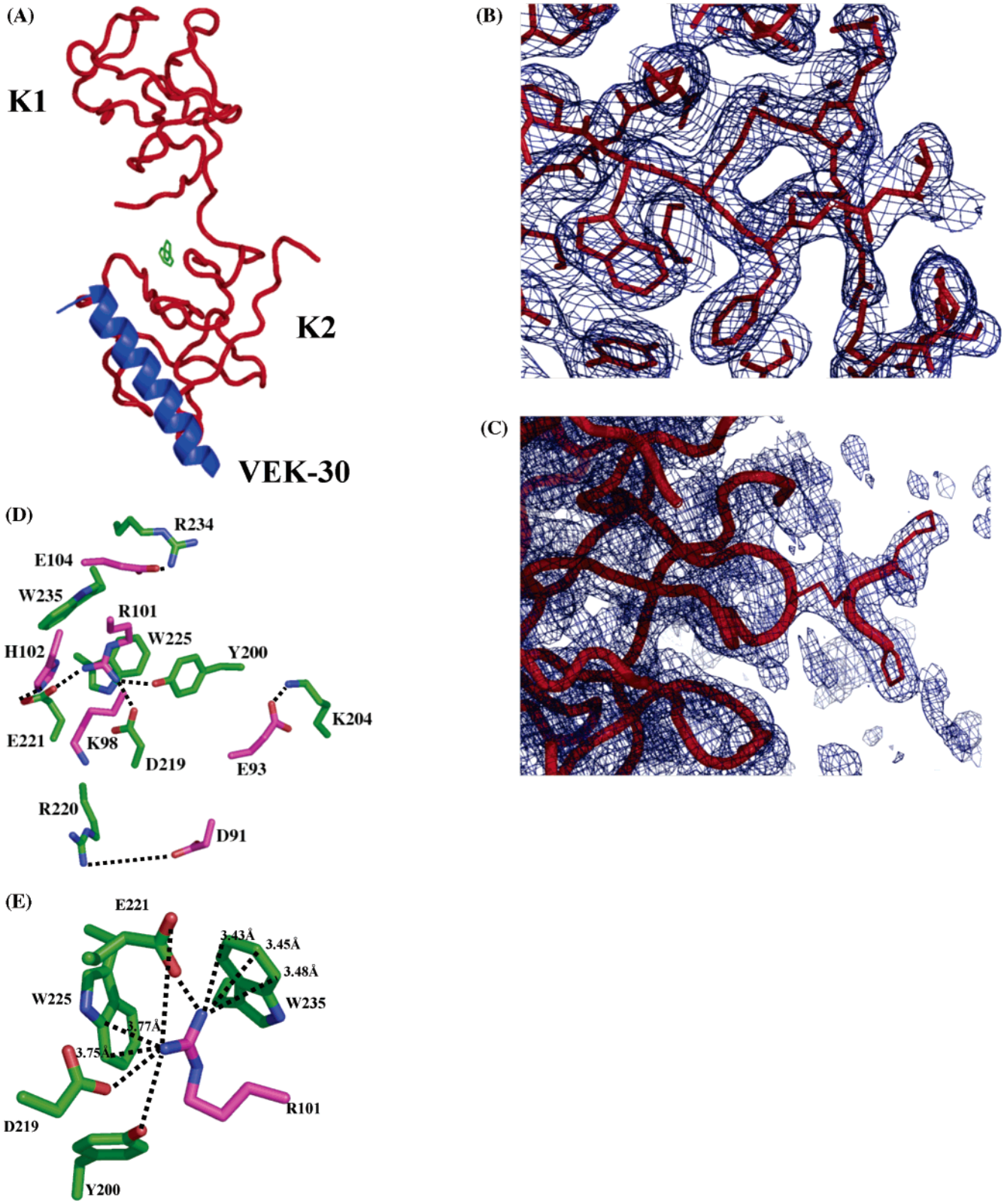

FIGURE 2: Structure of the angiostatin−VEK-30 complex. (A) Overall structure of the angiostatin−VEK-30 complex. Angiostatin is colored red, and VEK-30 is colored blue. One molecule of dioxane is colored green. (B) Example of a $2F_o - F_c$ map of the angiostatin−VEK-30 $P6_122$ structure contoured at 1σ. (C) Example of a $2F_o - F_c$ map of the angiostatin/VEK-30 $P6_1$ structure contoured at 1σ and centered at the inter-kringle K2−K3 disulfide bond (C169−C297). (D) Interaction between the angiostatin K2 LBS and VEK-30. R101 and E104 are spaced by almost one helical turn and form the through-space isostere for C-terminal lysine. Angiostatin is colored green, and VEK-30 is colored magenta. (E) Bidentate π−cation interaction occurs between the guanidino group of VEK-30 R101 and angiostatin K2 LBS residues W225 and W235. Angiostatin is colored green, and VEK-30 is colored magenta. All atoms are colored by atom type (nitrogen, blue; oxygen, red). Angiostatin residues are labeled with plasminogen numbering. VEK-30 residues are labeled with PAM numbering.

Interactions between VEK-30 and Angiostatin. Residues Glu93−Glu104 react with angiostatin (Figure 2D,E). This region encompasses most of the first direct repeat and the first residue of the second. Most of these interactions occur

Table 2: Interactions between Angiostatin and Vek-30 ($P6_122$ form)

angiostatin	VEK-30	distance (Å)
Y200 OH	L97 O	3.36
Y200 OH	K98 N	3.19
Y200 OH	R101 NH1	3.20
K204 NZ	E93 OE1	3.61
K204 NZ	E93 OE2	3.48
D219 OD1	R101 NH1	3.69
D219 OD2	R101 NH1	2.58
D219 O	K98 NZ	2.66
R220 NH1	D91 OD2	2.97
E221 OE1	R101 NH2	2.57
E221 OE1	H102 NE2	3.48
W225 NE1	R101 NH1	3.67
W225 CE2	R101 NH1	3.77
W225 CH2	R101 NE	3.80
W225 CH2	R101 CD	3.80
W225 CZ2	R101 NH1	3.75
W235 CD2	R101 NH2	3.43
W235 CE3	R101 NH2	3.41
W235 CZ3	R101 NH2	3.43
W235 CH2	R101 NH2	3.45
W235 CZ2	R101 NH2	3.48
R234 NH1	E104 OE1	3.15
W235 NE1	R101 O	3.15

between a single face of the helix and the K2 motif. One side of the helix consisting of residues K98−E104 makes numerous contacts with the angiostatin K2 LBS. Hydrogen bond and salt bridge electrostatic interactions occur between angiostatin K2 and VEK-30, both within and outside of the K2 LBS. There are no interactions between angiostatin K1 and VEK-30. The total number of contacts between angiostatin K2 and VEK-30 with a distance of <3.8 Å is ∼61. The LBS of the K2 domain contains consensus anionic (Asp219 and Glu221) and cationic (Arg234) centers (Figure 2D,E). VEK-30 forms a through-space isostere for C-terminal lysine by inserting residues Arg101 and Glu104 located on one face of the α-helix into the LBS of angiostatin K2. The principal interactions that occur between the anionic loci of the K2 LBS and VEK-30 involve residues Asp219 and Glu221 of K2 and Lys98, Arg101, and His102 of VEK-30. Critical salt bridge interactions occur between angiostatin K2 LBS residue Asp219 and VEK-30 residues Arg101 and Lys98. In addition, Glu221 makes a tight (distance of 2.57 Å) salt bridge contact with VEK-30 residue Arg101 and also makes contacts with His102 of VEK-30. A π−cation interaction also occurs between the guanidino group of Arg101 of VEK-30 and one of the two K2 Trp residues (Trp235) that make up the hydrophobic portion of the LBS (distances given in Table 2 and Figure 2E). At the cationic site, a salt bridge exists between residues Arg234 of K2 and Glu104 of VEK-30. An interaction between residues Arg220 of angiostatin and Asp91 of VEK-30 is also observed. VEK-30 Arg101 has proved to be vital for angiostatin K2 binding, since mutating this residue to Ala results in no measurable affinity for K2 (*19*). Mutating VEK-30 residues Lys98 and His102 to Ala and Glu104 to Gln results in a decreased affinity for the angiostatin K2 domain. These results suggest that the overall binding relies on interactions mediated by VEK-30 residues Lys98, Arg101, and His102 and are consistent with our crystallographic results.

There are also significant interactions between VEK-30 and K2 outside the LBS. A salt bridge interaction occurs between angiostatin K2 residue Lys204 and VEK-30 residue Glu93 (Figure 2D). It is unknown whether this exosite interaction is critical for binding. The exosite salt bridge interaction between angiostatin K2 residue Lys204 and VEK-30 residue Glu93 is further stabilized by hydrogen bonds and hydrophobic contacts of VEK-30 residues Leu94, Leu97, and Lys98 and angiostatin K2 residues Tyr200, Phe205, Asp219, and Arg220.

Most of the interactions discussed above are also seen in the structure of a mutated Pg K2 domain [K2(C169G/E221D/L237Y)] bound to VEK-30. However, two of the mutated residues, D221 and Y237, made interactions with VEK-30 in the LBS, calling into question whether the wild-type LBS would provide a similar interface. Our structure confirms that in spite of these mutations, most of the interface is similar in the two structures.

Kringle Domain Rotation. Comparison of the structures of unbound angiostatin to the VEK-30-bound form reveals that K1 has rotated significantly from its unbound conformation when the K2 regions are overlaid (Figure 3A). K1 of the angiostatin−VEK-30 complex rotates 48.1° and translates ∼0.5 Å from its position in the unbound angiostatin crystal structure [relative motion determined using DynDom (*44*)]. Residues encompassing the angiostatin K1−K2 linker peptide are the bending residues primarily responsible for such a large rotation. More specifically, the changes in ψ and ϕ dihedral angles of residues Glu163 and Glu165 contribute significantly to most of the interdomain rotation and are likely responsible for the large rotation of the angiostatin K1 domain seen in the angiostatin−VEK-30 structure. VEK-30 binding does not appear to be directly responsible for the rotation of K1 since there are no interactions between K1 and VEK-30. However, crystal packing dictates the K1 position in each structure indicating relative motion in solution. Angiostatin K1 clashes into a symmetry-related molecule of the angiostatin−VEK-30 complex when both K2 regions are overlaid. The same phenomenon is seen when K2 of the angiostatin−VEK-30 complex is overlaid onto angiostatin K2. This motion demonstrates that the kringle domains of angiostatin are not rigidly positioned as previously thought but are in fact mobile relative to each other. The LBS of Pg-K1 and Pg-K4 are known to play important roles in the maintenance of the closed conformation of Pg (*25*), although the involvement of the NTD with these binding sites is unclear. The fact that kringle domains of Pg are capable of significant structural rearrangement relative to one another indicates that transitions between the open and closed Pg conformations may also involve significant motion of K1−K3.

Kringle 3 Domain. A second $P6_1$ crystal form of the angiostatin−VEK-30 complex was produced by soaking crystals grown in the first, $P6_122$, form with Pt(II)-derivatizing molecules. This second crystal form preserves most of the crystal packing of the $P6_122$ form, although it loses the 2-fold axis perpendicular to the 6-fold axis. This results in a crystal form with two molecules in the asymmetric unit, instead of one. Though the structure of the complex is quite similar, several important differences are seen between the $P6_1$ and $P6_122$ crystal forms of the angiostatin−VEK-30 complex. In one molecule of the $P6_1$ structure, the inter-kringle disulfide bond is ordered. Residues Pro296, Cys297, and Lys298 of K3 are seen in the electron density, though no other residues of K3 were identified. This shows that the

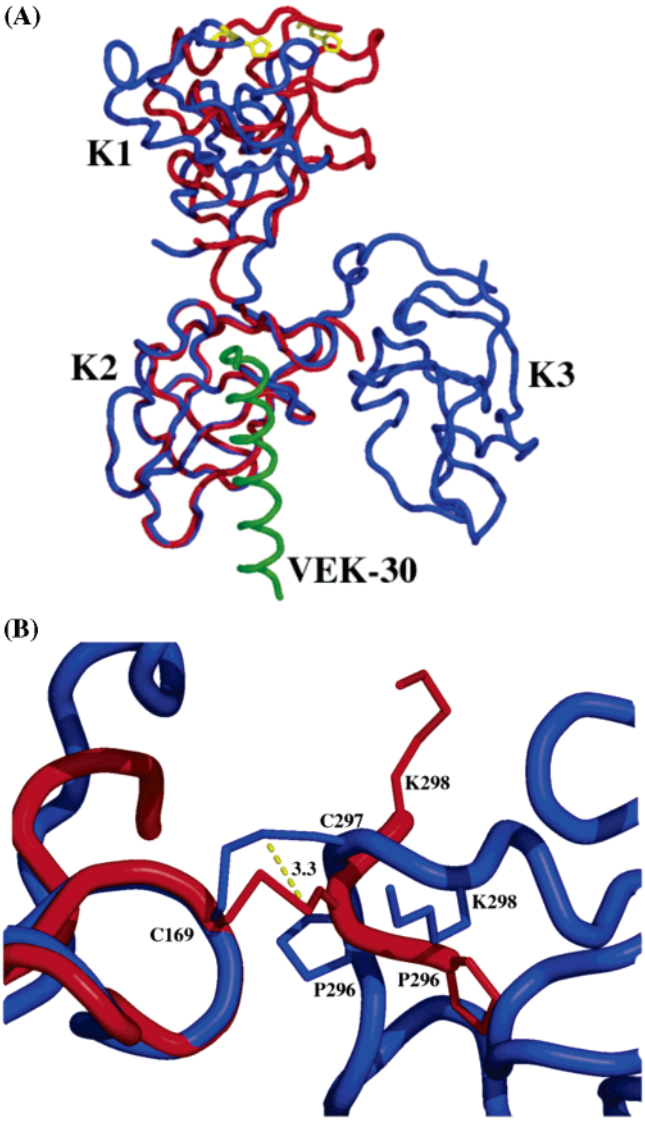

FIGURE 3: Pg kringles undergo significant structural rearrangement relative to one another. (A) Overlay of the K2 domains of the unliganded angiostatin and angiostatin−VEK-30 complex structures. The structure of angiostatin is colored blue, and the structure of the angiostatin−VEK-30 complex is colored red (angiostatin) and green (VEK-30). H114 of angiostatin is colored yellow in both structures. K1 of the angiostatin−VEK-30 complex undergoes a 48.1° rotation relative to the angiostatin structure. (B) Overlay of K2 of angiostatin with K2 of the angiostatin−VEK-30 complex from the $P6_1$ crystal form where three residues of angiostatin K3 are ordered. The $P6_1$ structure is colored red, and the structure of angiostatin is colored blue. The residues are labeled with Pg numbering. The inter-kringle disulfide bond in the $P6_1$ complex structure has rotated 3.3 Å from its position in the angiostatin structure.

K2−K3 inter-kringle disulfide bond remains intact in these structures, even though K3 appears to be disordered in the structures. Overlaying K2 of angiostatin with K2 of the angiostatin−VEK-30 complex in the $P6_1$ structure displays a significant motion of ∼3.3 Å at the inter-kringle disulfide bond (Figure 3B). When residues Pro296−Lys298 of the VEK-30-bound form are overlaid with the corresponding residues in the crystal structure of free angiostatin, one can see that angiostatin K3 encroaches upon a crystallographic symmetry-related molecule of K2. This indicates that there may be some structural differences within the angiostatin K3 domain to prevent steric clashes with a crystallographically related molecule. It should be noted that the conformation of the tripeptide alone fits in either structure. The motion of angiostatin K3 is limited due to the inter-kringle disulfide bond between residues Cys169 of K2 and Cys297 of K3. It has been suggested that the disruption of the K2−K3 inter-kringle disulfide bond is required for maximum angiogenic inhibition (*45*). However, the angiostatin double mutant (C169S/C297S), which eliminates the inter-kringle disulfide bond, has little effect on angiogenic activity but resulted in the loss of binding of EACA by K2, leading to the supposition that lysine binding by K2 was unimportant for anti-angiogenic activity (*46*). However, this loss of EACA binding is not in agreement with the binding of a series of α,ω-amino acids and VEK-30 to the C169G mutant of K2 (*47*) and the observation that the C169D/C297R double mutant retains the Cl^- and EACA-induced hydrodynamic properties of wild-type (WT) Pg (*25*). Similar conclusions regarding the irrelevance of binding of lysine to angiostatin were drawn from comparisons of lysine binding affinity and anti-angiogenic potency (*12*).

Dimerization. Inspection of the crystal packing indicated that dimerization between two angiostatin−VEK-30 complex molecules occurs along a crystallographic 2-fold axis (Figure 4A). The same dimerization was seen in the K2−VEK-30 structure between the two K2−VEK-30 molecules in the asymmetric unit (*19*). This indicates that dimerization is not an artifact of crystal packing since there is obviously no relationship between the crystal packing in the K2−VEK-30 complex and the angiostatin−VEK-30 complex. The Cα positions of the dimeric structure of the K2−VEK-30 complex superimpose well with the two angiostatin−VEK-30 complexes that are related by crystallographic 2-fold symmetry (rmsd for all atoms of ∼0.4 Å). Dimerization results in two molecules of α-helical VEK-30 packing parallel and side by side in the center of the dimer and two K2 domains located on either side of the parallel helices. Interestingly, full-length PAM is predicted to homodimerize as a coiled coil that extends on either side of the VEK-30 region (*48*). In fact, several homology modeling programs predict the PAM structure based on the extended coiled-coil structure of tropomyosin (*48*, *49*). The only region of PAM (between amino acids 60 and 310) that is not well-fitted by the coiled-coil structural prediction is the Pg-binding direct repeat region that encompasses the VEK-30 peptide (W. Wedemeyer, unpublished results). This is consistent with the structure of the angiostatin−VEK-30 dimer in that the two helices do not form a classical coiled coil, though they are parallel and stacked side to side. Numerous contacts between the two molecules at the dimerization interface are observed. As shown in Figure 4B, water-mediated interactions occur at the dimerization interface between angiostatin K2 residue Gln193 of the symmetry-related molecule and VEK-30 residue Asn99. Another water-mediated interaction occurs at angiostatin K204 and VEK-30 Glu94. Numerous hydrogen bonds also play a role at the dimerization interface. Hydrogen bonds occur between VEK-30 residue Glu103 and angiostatin K2 symmetry-related molecule residues His196 and Ala197. Another hydrogen bond occurs between VEK-30 residue E100 and angiostatin symmetry-related molecule Arg234, the cationic site within the K2 LBS. The calculated total buried surface area of a dimer of the angiostatin−VEK-30 complex is 1627 $Å^2$, suggesting a relatively strong

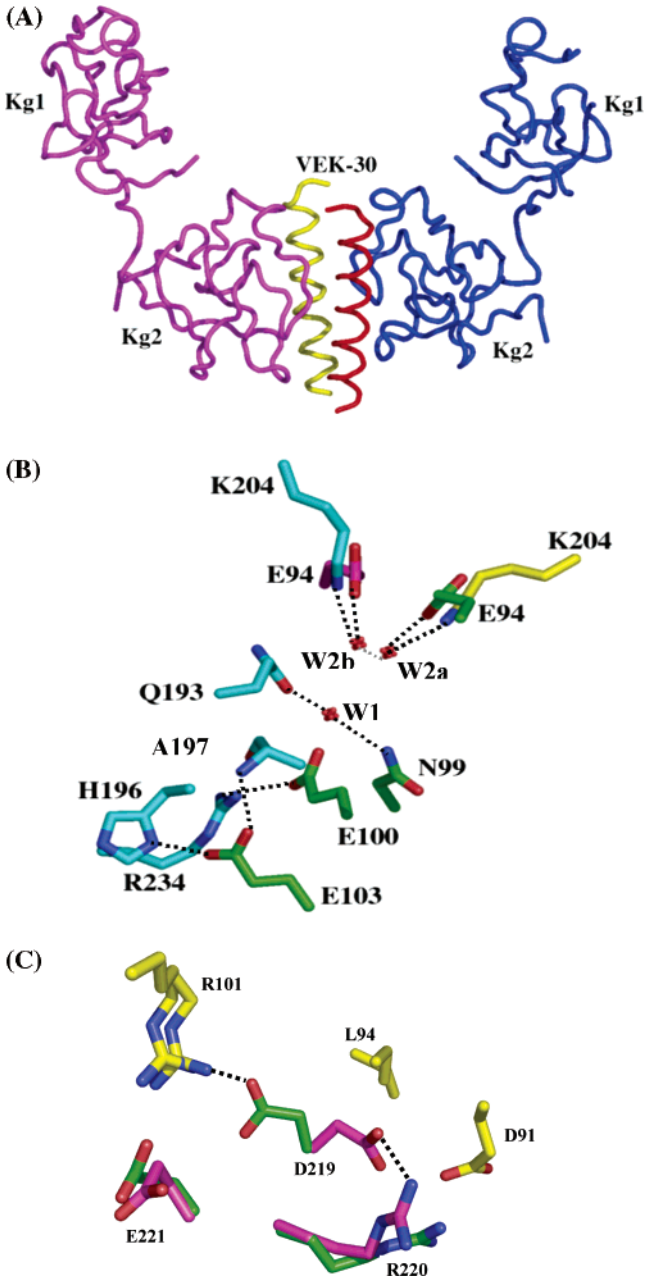

FIGURE 4: Dimerization occurs in the angiostatin−VEK-30 complex structure. (A) Dimerization of the angiostatin−VEK-30 complex. One molecule has angiostatin colored blue and VEK-30 colored red, while the other molecule has angiostatin colored magenta and VEK-30 colored yellow. (B) Residues involved in dimerization. VEK-30 residues are colored green, and angiostatin K2 residues are colored yellow. The symmetry-related molecule of angiostatin K2 is colored cyan with its VEK-30 residue colored magenta. The atoms are colored by type. The water molecules are designated as W1 and the symmetry-related waters as W2a and W2b. All residues are labeled with Pg and PAM numbering. (C) Overlay of angiostatin K2 onto angiostatin−VEK-30 complex K2. Residues from angiostatin alone are colored magenta; residues from the angiostatin−VEK-30 complex are colored green, and VEK-30 residues are colored yellow. The atoms are colored by type. All residues are labeled with Pg and PAM numbering. D219 is flipped out of the LBS, resulting in a tight salt bridge contact with R220.

interaction. Furthermore, because a dimeric structure is exhibited by both K2−VEK-30 and angiostatin−VEK-30 complexes, it is plausible that such higher-order structures may exist in solution. To address this possibility, sedimentation equilibrium analysis was conducted on angiostatin in the absence and presence of VEK-30. The apparent molecular weight of angiostatin (at a concentration of 13 μM) was determined to be 27 700 ± 100 (calculated sequence-based weight of 29 000). In the presence of a 5-fold molar excess of VEK-30 [allowing for virtually all angiostatin to exist in VEK-30-bound form assuming a K_d of 460 nM for the angiostatin−VEK-30 interaction (*47*)], an apparent molecular weight of 28 400 ± 800 was obtained. These data fail to support a model of VEK-30-mediated dimerization of angiostatin at angiostatin concentrations that are physiologically feasible based on circulating plasma levels (ca., 2 μM) of the Pg parent (*50*). However, this does not rule out the possibility of a PAM-induced angiostatin (or Pg) dimer on the bacterial surface, where high effective concentrations of both binding partners can be encountered and where full-length PAM is strongly predicted to exist as a parallel coiled-coil dimer, as are all proteins in the M protein family (*48*, *49*).

Kringle 2 Domain Specificity. The Pg kringles have high degrees of sequence and structural homology. However, the Pg kringles are very different with respect to their affinity for C-terminal lysine mimics and in their biological functions in proliferation and migration assays. A closer examination of the residues of K2 involved in VEK-30 interactions reveals that many of these residues are not conserved in Pg kringle domains. For instance, Gln193 is responsible for mediating interactions at the angiostatin−VEK-30 dimerization interface. In K1 and K4, this sequence position is occupied by Thr and Met, respectively. Ala197 of K2 is not conserved in Pg kringle domains and also plays a role at the dimerization interface (K1, K4, and K5 all have Arg residues while K3 has a Thr). K2 residue Lys204 is also not conserved and is involved in mediating interactions at the dimerization interface, as well as directly interacting with VEK-30 through an exosite region. If we focus on residues within the LBS, Y200 is not conserved whereas K1 and K5 have Phe and K3 and K4 have Arg and Lys, respectively. Tyr200 of K2 forms numerous interactions with VEK-30. Specifically, the hydroxyl group of Tyr200 makes a hydrogen bond with the NH1 atom of Arg101. Finally, Arg220 makes contacts with VEK-30, and this site is also not conserved in Pg kringle domains. Specifically, Arg220 forms a salt bridge with Asp219 in the angiostatin structure. Because of the interaction with Arg220, Asp219 is flipped out of the LBS and is incapable of interacting with the C-terminal group of EACA, possibly explaining the poor EACA binding affinity of K2 (*5*−*7*, *12*, *51*). However, VEK-30 abrogates the salt bridge interaction between Arg220 and Asp219 so that Asp219 flips into the LBS. This rearrangement recapitulates the canonical LBS architecture, permitting extensive LBS−VEK-30 interactions (Figure 4C). Mouse Pg has a substantially lower affinity for PAM than human Pg does, although the two domains are 86% identical in sequence. Arg220 is the only residue that both interacts, either directly or indirectly, with VEK-30 and is not identically conserved in mouse Pg. This strongly implicates Arg220 as a residue that is both important for binding and critical to the species specificity of PAM. In summary, many of the K2 residues that interact with VEK-30 are not conserved among Pg-K1, -K3, -K4, and -K5, likely explaining why only human Pg-K2 has affinity for VEK-30. The sequence analysis results identify potential targets for further mutagenesis studies.

DISCUSSION

The angiostatin−VEK-30 structure is the only interaction between a multiple-kringle protein and a ligand to be characterized and is the sole model for complexation of angiostatin with its cognate protein-binding partners. Interestingly, other known angiostatin protein ligands, $\alpha_v\beta_3$ integrin and F_1-F_0 ATP synthase, both contain a possible through-space isostere for C-terminal lysine similar to that of VEK-30 (*12*). However, data defining the interface between angiostatin and these targets have not yet been reported.

The complex between VEK-30 and angiostatin suggests a possible mechanism for Pg activation during group A streptococci infection. SK is secreted by group A streptococci and activates human Pg (*2*, *3*). It does so by binding to the catalytic domain of Pg, causing a conformational change in Pg within the complex that results in formation of an active site in the bound Pg (SK−Pg′). This SK−Pg′ complex activates other molecules of Pg or is converted to SK−Pm, another potent Pg activator. Previous studies have shown that both SK and PAM contribute to virulence during group A streptococci impetigo (*52*). Specifically, "molecular cooperation" between SK and PAM occurs, resulting in the bacterial acquisition of the host Pm so that the pathogen is able to invade host tissues (*53*). Previous experiments suggest that streptokinase activates PAM-bound Pg and also preferentially binds the open form of Pg (*30*). Our structure of the angiostatin−VEK-30 complex suggests that the PAM region might induce the open conformation of Pg on the cell surface by altering the relative orientation of the Pg kringle domains and by steric interference between its extended helical structure and Pg. Although VEK-30-mediated dimerization was not observed under physiologically relevant solution conditions, this does not rule out dimerization of Pg by full-length PAM on the bacterial cell surface. This dimerization may also promote a Pg conformation that is more amenable to SK binding and would also bring two molecules of Pg together on the cell surface. Binding of SK to one Pg could then result in proximity-accelerated activation of the second.

ACKNOWLEDGMENT

We thank W. Wedemeyer for helpful discussions and his assistance in homology modeling the full-length PAM structure.

REFERENCES

1. Ploplis, V. A., and Castellino, F. J. (2000) Nonfibrinolytic functions of plasminogen, *Methods 21*, 103−110.
2. Castellino, F. J. (1984) Biochemistry of human plasminogen, *Semin. Thromb. Haemostasis 10*, 18−23.
3. Ponting, C. P., Marshall, J. M., and Cederholm-Williams, S. A. (1992) Plasminogen: A structural review, *Blood Coagulation Fibrinolysis 3*, 605−614.
4. Castellino, F. J., and Ploplis, V. A. (2005) Structure and function of the plasminogen/plasmin system, *Thromb. Haemostasis 93*, 647−654.
5. Urano, T., Deserrano, V. S., Chibber, B. A. K., and Castellino, F. J. (1987) The Control of the Urokinase-Catalyzed Activation of Human Glutamic-Acid 1-Plasminogen by Positive and Negative Effectors, *J. Biol. Chem. 262*, 15959−15964.
6. Urano, T., Chibber, B. A. K., and Castellino, F. J. (1987) The Reciprocal Effects of ϵ-Aminohexanoic Acid and Chloride-Ion on the Activation of Human [Glu1]Plasminogen by Human Urokinase, *J. Biol. Chem. 84*, 4031−4034.
7. Winn, E. S., Hu, S. P., Hochschwender, S. M., and Laursen, R. A. (1980) Studies on the lysine-binding sites of human plasminogen. The effect of ligand structure on the binding of lysine analogs to plasminogen, *Eur. J. Biochem. 104*, 579−586.
8. Mathews, I. I., Vanderhoff-Hanaver, P., Castellino, F. J., and Tulinsky, A. (1996) Crystal structures of the recombinant kringle 1 domain of human plasminogen in complexes with the ligands ϵ-aminocaproic acid and trans-4-(aminomethyl)cyclohexane-1-carboxylic acid, *Biochemistry 35*, 2567−2576.
9. McCance, S. G., Menhart, N., and Castellino, F. J. (1994) Amino-Acid-Residues of the Kringle-4 and Kringle-5 Domains of Human Plasminogen That Stabilize Their Interactions with ω-Amino Acid Ligands, *J. Biol. Chem. 269*, 32405−32410.
10. Chang, Y., Mochalkin, I., McCance, S. G., Cheng, B. S., Tulinsky, A., and Castellino, F. J. (1998) Structure and ligand binding determinants of the recombinant kringle 5 domain of human plasminogen, *Biochemistry 37*, 3258−3271.
11. Wu, T. P., Padmanabhan, K., Tulinsky, A., and Mulichak, A. M. (1991) The refined structure of the ϵ-aminocaproic acid complex of human plasminogen kringle 4, *Biochemistry 30*, 10589−10594.
12. Geiger, J. H., and Cnudde, S. E. (2004) What the structure of angiostatin may tell us about its mechanism of action, *J. Thromb. Haemostasis 2*, 23−34.
13. Clemmensen, I., Petersen, L. C., and Kluft, C. (1986) Purification and characterization of a novel, oligomeric, plasminogen kringle 4 binding protein from human plasma: Tetranectin, *Eur. J. Biochem. 156*, 327−333.
14. Graversen, J. H., Lorentsen, R. H., Jacobsen, C., Moestrup, S. K., Sigurskjold, B. W., Thogersen, H. C., and Etzerodt, M. (1998) The plasminogen binding site of the C-type lectin tetranectin is located in the carbohydrate recognition domain, and binding is sensitive to both calcium and lysine, *J. Biol. Chem. 273*, 29241−29246.
15. Graversen, J. H., Sigurskjold, B. W., Thogersen, H. C., and Etzerodt, M. (2000) Tetranectin-binding site on plasminogen kringle 4 involves the lysine-binding pocket and at least one additional amino acid residue, *Biochemistry 39*, 7414−7419.
16. Schenone, M. M., Warder, S. E., Martin, J. A., Prorok, M., and Castellino, F. J. (2000) An internal histidine residue from the bacterial surface protein, PAM, mediates its binding to the kringle-2 domain of human plasminogen, *J. Pept. Res. 56*, 438−445.
17. Wistedt, A. C., Ringdahl, U., Muller-Esterl, W., and Sjobring, U. (1995) Identification of a plasminogen-binding motif in PAM, a bacterial surface protein, *Mol. Microbiol. 18*, 569−578.
18. Wistedt, A. C., Kotarsky, H., Marti, D., Ringdahl, U., Castellino, F. J., Schaller, J., and Sjobring, U. (1998) Kringle 2 mediates high affinity binding of plasminogen to an internal sequence in streptococcal surface protein PAM, *J. Biol. Chem. 273*, 24420−24424.
19. Rios-Steiner, J. L., Schenone, M., Mochalkin, I., Tulinsky, A., and Castellino, F. J. (2001) Structure and binding determinants of the recombinant kringle-2 domain of human plasminogen to an internal peptide from a group A streptococcal surface protein, *J. Mol. Biol. 308*, 705−719.
20. Suenson, E., and Thorsen, S. (1981) Secondary-Site Binding of Glu-Plasmin, Lys-Plasmin and Miniplasmin to Fibrin, *Biochem. J. 197*, 619−628.
21. Christensen, U., and Molgaard, L. (1992) Positive co-operative binding at two weak lysine-binding sites governs the Glu-plasminogen conformational change, *Biochem. J. 285* (Part 2), 419−425.
22. Takada, Y., Urano, T., and Takada, A. (1993) Conformational change of plasminogen: Effects of N-terminal peptides of Glu-plasminogen, *Thromb. Res. 70*, 151−159.
23. Mangel, W. F., Lin, B., and Ramakrishnan, V. (1990) Characterization of an Extremely Large, Ligand-Induced Conformational Change in Plasminogen, *Science 248*, 69−73.
24. Marshall, J. M., Brown, A. J., and Ponting, C. P. (1994) Conformational Studies of Human Plasminogen and Plasminogen Fragments: Evidence for a Novel 3rd Conformation of Plasminogen, *Biochemistry 33*, 3599−3606.
25. McCance, S. G., and Castellino, F. J. (1995) Contributions of individual kringle domains toward maintenance of the chloride-induced tight conformation of human glutamic acid-1 plasminogen, *Biochemistry 34*, 9581−9586.

26. Cockell, C. S., Marshall, J. M., Dawson, K. M., Cederholm-Williams, S. A., and Ponting, C. P. (1998) Evidence that the conformation of unliganded human plasminogen is maintained via an intramolecular interaction between the lysine-binding site of kringle 5 and the N-terminal peptide, *Biochem. J. 333* (Part 1), 99−105.
27. Berge, A., and Sjobring, U. (1993) PAM, a Novel Plasminogen-binding Protein from *Streptococcus pyogenes*, *J. Biol. Chem. 268*, 25417−25424.
28. Fischetti, V. A. (1989) Streptococcal M protein: Molecular design and biological behavior, *Clin. Microbiol. Rev. 2*, 285−314.
29. Sanderson-Smith, M., Batzloff, M., Sriprakash, K., Dowton, M., Ranson, M., and Walker, M. (2006) Divergence in the plasminogen-binding group A streptococcal M protein family: Functional conservation of binding site and potential role for immune selection of variants, *J. Biol. Chem. 281*, 3217−3226.
30. Boxrud, P. D., and Bock, P. E. (2000) Streptokinase binds preferentially to the extended conformation of plasminogen through lysine binding site and catalytic domain interactions, *Biochemistry 39*, 13974−13981.
31. Phillips, G. J., Flicker, P., Cohen, C., Manjula, B., and Fischetti, V. A. (1981) Streptococcal M protein: α-Helical coiled-coil structure and arrangement on the cell surface, *Proc. Natl. Acad. Sci. U.S.A. 78*, 4689−4693.
32. O'Reilly, M. S., Holmgren, L., Shing, Y., Chen, C., Rosenthal, R. A., Moses, M., Lane, W. S., Cao, Y., Sage, E. H., and Folkman, J. (1994) Angiostatin: A novel angiogenesis inhibitor that mediates the suppression of metastases by a Lewis lung carcinoma, *Cell 79*, 315−328.
33. O'Reilly, M. S., Holmgren, L., Shing, Y., Chen, C., Rosenthal, R. A., Cao, Y., Moses, M., Lane, W. S., Sage, E. H., and Folkman, J. (1994) Angiostatin: A circulating endothelial cell inhibitor that suppresses angiogenesis and tumor growth, *Cold Spring Harbor Symp. Quant. Biol. 59*, 471−482.
34. Folkman, J. (1995) Angiogenesis in cancer, vascular, rheumatoid and other disease, *Nat. Med. 1*, 27−31.
35. Folkman, J., and Shing, Y. (1992) Angiogenesis, *J. Biol. Chem. 267*, 10931−10934.
36. MacDonald, N. J., Murad, A. C., Fogler, W. E., Lu, Y. Y., and Sim, B. K. L. (1999) The tumor-suppressing activity of angiostatin protein resides within kringles 1 to 3, *Biochem. Biophys. Res. Commun. 264*, 469−477.
37. Shepard, S. R., Boucher, R., Johnston, J., Boerner, R., Koch, G., and Madsen, J. (2000) Large-scale purification of recombinant human angiostatin, *Protein Expression Purif. 20*, 216−227.
38. Otwinowski, Z. (1993) *Oscillation data reduction program*, SERC Daresbury Laboratory, Warrington, U.K.
39. Navaza, J. (1994) AMoRe, an automated program for molecular replacement, *Acta Crystallogr. A50*, 157−163.
40. Otwinowski, Z., and Minor, W. (1997) Processing of X-ray diffraction data collected in oscillation mode, *Methods Enzymol. 276*, 307−326.
41. Terwilliger, T. C., and Berendzen, J. (1999) Automated MAD and MIR structure solution, *Acta Crystallogr. D55*, 849−861.
42. Collaborative Computational Project, Number 4 (1994) The CCP4 Suite: Programs for Protein Crystallography, *Acta Crystallogr. D50*, 760−763.
43. Brunger, A. T., Adams, P. D., Clore, G. M., DeLano, W. L., Gros, P., and Grosse-Kuntsleve, R. W. (1998) Crystallography & NMR System: A new software suite for macromolecular structure determination, *Acta Crystallogr. D54*, 905−921.
44. Hayward, S., and Berendsen, H. J. C. (1998) Systematic Analysis of Domain Motions in Proteins from Conformational Change: New Results on Citrate Synthase and T4 Lysozyme, *Proteins: Struct., Funct., Genet. 30*, 144.
45. Cao, Y., Ji, R. W., Davidson, D., Schaller, J., Marti, D., Sohndel, S., McCance, S. G., O'Reilly, M. S., Llinas, M., and Folkman, J. (1996) Kringle domains of human angiostatin. Characterization of the anti-proliferative activity on endothelial cells, *J. Biol. Chem. 271*, 29461−29467.
46. Lee, H., Kim, H. K., Lee, J. H., You, W. K., Chung, S. I., Chang, S. I., Park, M. H., Hong, Y. K., and Joe, Y. A. (2000) Disruption of interkringle disulfide bond of plasminogen kringle 1-3 changes the lysine binding capability of kringle 2, but not its antiangiogenic activity, *Arch. Biochem. Biophys. 375*, 359−363.
47. Nilsen, S. L., Prorok, M., and Castellino, F. J. (1999) Enhancement through mutagenesis of the binding of the isolated kringle 2 domain of human plasminogen to σ-amino acid ligands and to an internal sequence of a streptococcal surface protein, *J. Biol. Chem. 274*, 22380−22386.
48. Jones, D. (1998) THREADER: Protein Sequence Threading by Double Dynamic Programming., in *Computational Methods in Molecular Biology* (Salzberg, S., Searls, D., and Kasif, S., Eds.) Elsevier Science, Amsterdam.
49. Whitby, F., and Phillips, G., Jr. (2000) Crystal structure of tropomyosin at 7 Å resolution, *Proteins 38*, 49−59.
50. Collen, D., and Lijnen, H. R. (1991) Basic and clinical aspects of fibrinolysis and thrombolysis, *Blood 78*, 3114−3124.
51. Abad, M. C., Arni, R. K., Grella, D. K., Castellino, F. J., Tulinsky, A., and Geiger, J. H. (2002) The X-ray crystallographic structure of the angiogenesis inhibitor angiostatin, *J. Mol. Biol. 318*, 1009−1017.
52. Svensson, M. D., Sjobring, U., Luo, F., and Bessen, D. E. (2002) Roles of the plasminogen activator streptokinase and the plasminogen-associated M protein in an experimental model for streptococcal impetigo, *Microbiology 148*, 3933−3945.
53. Ringdahl, U., Svensson, M., Wistedt, A. C., Renn, T., Kellner, R., Muller-Esterl, W., and Sjobring, U. (1998) Molecular cooperation between protein PAM and streptokinase for plasmin acquisition by *Streptococcus pyogenes*, *J. Biol. Chem. 272*, 6424−6230.

BI060914J